Numerical Simulation on Asymmetrical Interface of Floating Zone (FZ) for Silicon Crystal Growth

HAN, Xue-Feng
Research Institute for Applied Mechanics, Kyushu University

LIU, Xin
Research Institute for Applied Mechanics, Kyushu University

Nakano, Satoshi
Research Institute for Applied Mechanics, Kyushu University

Harada, Hirofumi
Research Institute for Applied Mechanics, Kyushu University

他

https://doi.org/10.15017/1957534

出版情報：九州大学応用力学研究所所報. 155, pp.11-16, 2018-09. Research Institute for Applied Mechanics, Kyushu University
バージョン：
権利関係：

Numerical Simulation on Asymmetrical Interface of Floating Zone (FZ) for Silicon Crystal Growth

Xue-Feng HAN[*1], Xin LIU[*1], Satoshi NAKANO[*1],
Hirofumi HARADA[*1] , Yoshiji MIYAMURA[*1] and Koichi KAKIMOTO[*1]
E-mail of corresponding author: *han0459@riam.kyushu-u.ac.jp*

(Received August 29, 2018)

Abstract

A three-dimensional global heat transfer model has been developed to describe the floating zone of silicon single-crystal growth. The calculations of argon gas flow, feed rod, silicon melt and crystal are carried out using open-source software OpenFOAM. In order to investigate the asymmetrical phenomena during the growth process, no assumption of axis-symmetric has been made. Three-dimensional electromagnetic field has been calculated. It is confirmed that solid-liquid interface is not symmetric. From the calculation results, it is concluded that asymmetric melt flow and asymmetric interface under the current supplier are caused by the asymmetric inductor.

Keywords : *Floating zone, Silicon, Computational fluid dynamics*

1. Introduction

Floating zone (FZ) method is the most popular method for the growth of high-purity monocrystalline silicon applying to voltage power electronic equipment [1], as it avoids crucible contamination during the growth process. The quality of power electronic equipment largely depends on the crystal quality. The azimuthal growth-rate fluctuations greatly influence the impurity striations [2]. Two-dimensional (2D) calculations and experimental results obtained by using the needle-eye technique have been compared in the previous study [3, 4]. However, asymmetric electromagnetic (EM) field caused by the inductor current supplier is not considered due to the axis-symmetry of the model. 3D convection flow and temperature field are calculated by using FEMAG and COMSOL [5, 6]. 2D global model is used from the specialized program FZone with the 3D local model from OpenFOAM to investigate the interface, gas flow, and melt flow [7–9]. However, asymmetric deflection of the interface in a 3D global model has not been discussed.

We thus focus in the present paper on studying the asymmetric shape of the 3D interface during crystal growth by developing a full 3D global model. To analyze how the asymmetric inductor affects the shape of the interface, we calculate the 3D EM field in the furnace. Since the cooling effect of the gas is also important to the temperature field, the

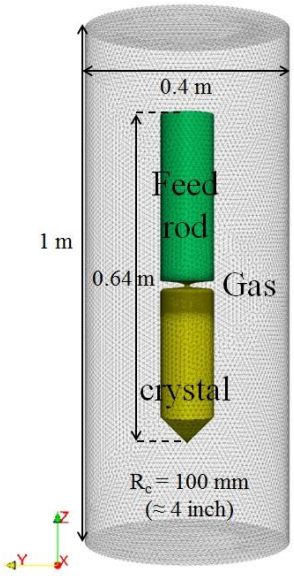

Fig.1 Three-dimenstional global model of the FZ system for 4-inch single crystal silicon: feed rod, melt, crystal and gas. The total height of the furnace is 1 m. the diameter of the furnace is 0.4 m.

*1 Research Institute for Applied Mechanics, Kyushu Univ.

ambient gas is also considered 3D. Because the temperature at the melt surface is not homogenous, Marangoni effect is also considered in the melt model.

2. Numerical models

Fig. 1 shows the 3D global model developed by using the open-source mesh program SALOME [10]. The crystal is aussumed as 100 mm (4 inches) in diameter. The total length of the crystal and feed rod is 0.64 m. The calculation was conducted with FzGlobalFOAM, which was developed based on the open-source libarry OpenFOAM 2.3.1 [11]. Fig. 2 shows the calculation algorithm in the model. The calculation starts from the Current supplier boundary condition. The initial voltage between the electrodes is set to 1V. From the current density distribution, the EM field can be obtained. After calculating the EM field, gas flow, melt flow and temperature have been calculated. If the temperature at the three-phase point is different from the melting point, the heating power density will be scaled and iterated until the result converges. The mesh is made up of more than 2 million tetrahedral cells. To verify the accuracy of the mesh, two additional models have been compared. The number of cells are 59 million and 95 million, respectively. When the cell number is larger than 950,000, there is no obvious mesh dependence. 2 million mesh is used for the smoothness of the interface.

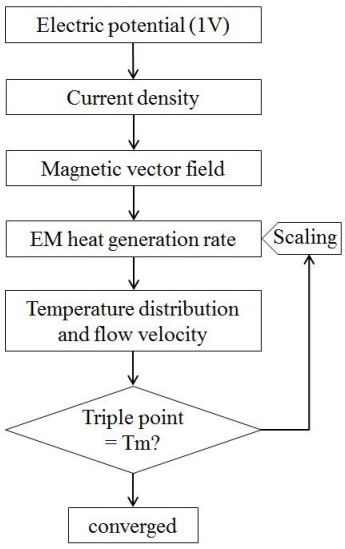

Fig.2 Flowchart of the global calculation.

In the actual process, the heating power density and temperature distribution at the free surface are not symmetric due to the design of needle-eye inductor. Therefore, the influence of the asymmetric inductor should be considered. Fig. 3 shows the geometry of the inductor which consists of separate current suppliers, one main slit, and three side slits. The electric field $\boldsymbol{E}$ is regarded as uniform, it can be derived by the following equation:

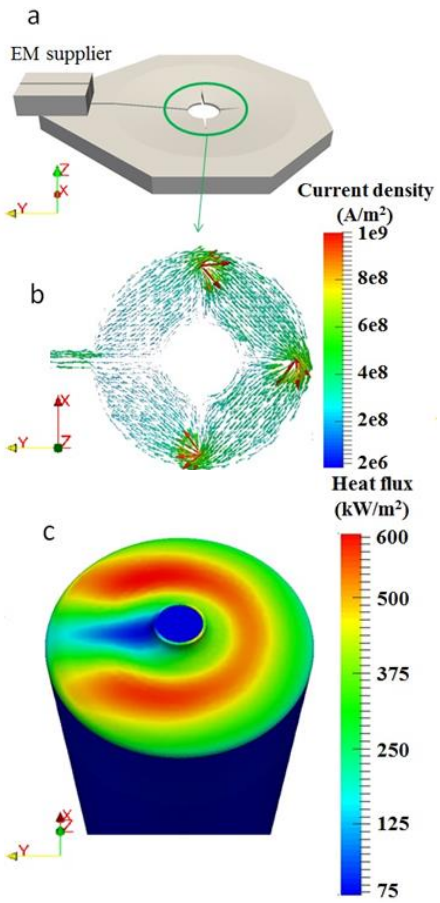

Fig.3 (a) Model of inductor design (b) Current density distribution in the inductor. (c) Heat generation rate at the free surface of melt induced by inductor.

$$\boldsymbol{E} = -\boldsymbol{\nabla}(\varphi) \tag{1}$$

From Ohm's law, the current density $\boldsymbol{J}$ is calculated by

$$\boldsymbol{J} = \sigma_c \boldsymbol{E} \tag{2}$$

Here, σ_c is electrical conductivity. The current density $\boldsymbol{J}$ is coupled with magnetic field. And the magnetic vector potential $\boldsymbol{A}$ given by [12]

$$\nabla^2 \boldsymbol{A} = -\mu \boldsymbol{J} \tag{3}$$

where μ is the permeability of free space. The heat generation rate Q_{EM} at the free surface is calculated by

$$Q_{EM} = \frac{\sigma_s \omega^2 \boldsymbol{A}^2}{2} \tag{4}$$

where σ_s and ω are the electrical conductivity of the molten silicon and the angular frequency of the EM field, respectively.

The melt temperature also can be influenced by the heat transfer of gas. the gas is assumed to be a compressible fluid

since its properties are changed with temperature. Argon gas can be modeled by the folloing equation:

$$\rho = \frac{PM_w}{RT} \tag{5}$$

ρ is the gas density, P is the gas pressure, M_w is molar mass of the gas, R is the universal gas constant, and T is the absolute temperature. The steady-state flow are calculated by the continuity and Navier–Stokes equations:

$$\nabla(\rho \boldsymbol{U}) = 0 \tag{6}$$

$$\nabla(\rho \boldsymbol{U}\boldsymbol{U}) = \nabla(\mu_{\text{eff}} \nabla \cdot \boldsymbol{U}) - \nabla P + \rho \boldsymbol{g} \tag{7}$$

where $\boldsymbol{U}$ is the velocity vector, μ_{eff} is the viscosity (including the effects of turbulence), and g is gravity vector.

Because the speed of rotation and the speed of pulling are lower than the speed of air flow, all the boundaries of the gas field are assumed to be steady, which are considered as non-slip walls. For the current conditions, since the Reynolds number of argon gas is much larger than the onset value of turbulence, the default shear stress transfer (SST) k-turbulence model [13] is used in the calculation. The inlet and outlet of the furnace are not included to ensure the stability of the calculation. The pressure is 1 bar. Radiantion heat transfer from feed rod, melt and crystal is calculated by using P1 model. The radiantion heat flux calculated by the P1 model is coupled with the energy equations of feed, melt and crystal.

The steady-state melt flow is modeled by using the Boussinesq approximation with the solidification model. At the melt free surface, the Marangoni force is considered. The surface force $\boldsymbol{F}$ caused by surface tension change is given by

$$\boldsymbol{F} = \frac{\partial \gamma}{\partial T} \nabla T \tag{8}$$

Here, $\partial\gamma/\partial T$ is the surface tension coefficient as a function of temperature. The other boundaries for the melt are designated as non-slip walls. The steady-state heat transfer in the melt is modeled by the enthalpy equation:

$$\nabla \cdot \left(\rho \boldsymbol{U} h + \frac{\rho \boldsymbol{U}^2}{2} \right) = \nabla \cdot (a \nabla h) \tag{9}$$

where h is enthalpy and a is thermal diffusivity, which is defined as the ratio of viscosity μ_v to Prandtl number Pr:

$$a = \mu_v / Pr \tag{10}$$

Moreover, the temperature of the melt boundaries is coupled with the feed, crystal, and gas domains. The heat generation rate of solidification Q_L is considered as a function of growth rate V_g:

$$Q_L = \rho V_g L \tag{11}$$

where L is the latent heat of silicon. The heat generation of solidification rate Q_L and heat generation rate Q_{EM} are added into the enthalpy equation (9) as source terms.

3. Results and discussion

The existence of current supplier makes the inductor asymmetric, which causes an asymmetric distribution of current density inside the inductor. Fig. 3(b) shows the current-density distribution at the plane of the effective part of the inductor. The current density is small at the main slit. The asymmetric current density also leads to an asymmetric

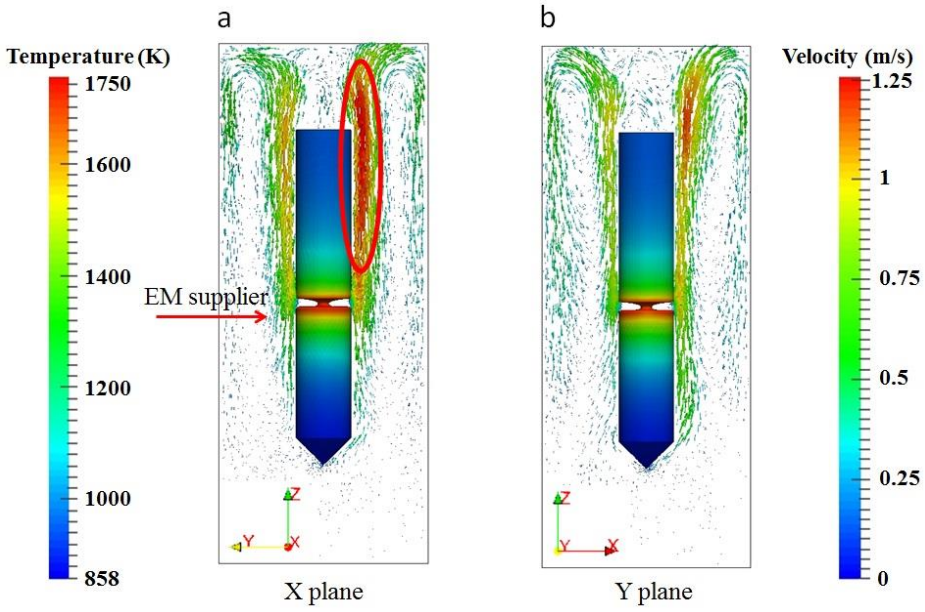

Fig.4 Temperature distribution and velocity vector distribution of gas flow at cross section: (a) X plane; (b) Y plane

distribution of the EM heat generation rate. Fig. 3(c) shows the heat flux density caused by the EM field at the free surface of the melt domain. Below the main slit of the inductor, the minimum heat flux induced by the EM field occurs.

3D steady-state calculation of gas flow is used to account for the effect of gas flow on the temperature of the feed rod, melt, and crystal. The gas flow is decided by the temperature gradient of the feed rod, melt, and crystal. By comparing the gas flow velocity distribution in the X plane [Fig. 4(a)] to that in the Y plane [Fig. 4(b)], it is investigated that the maximum

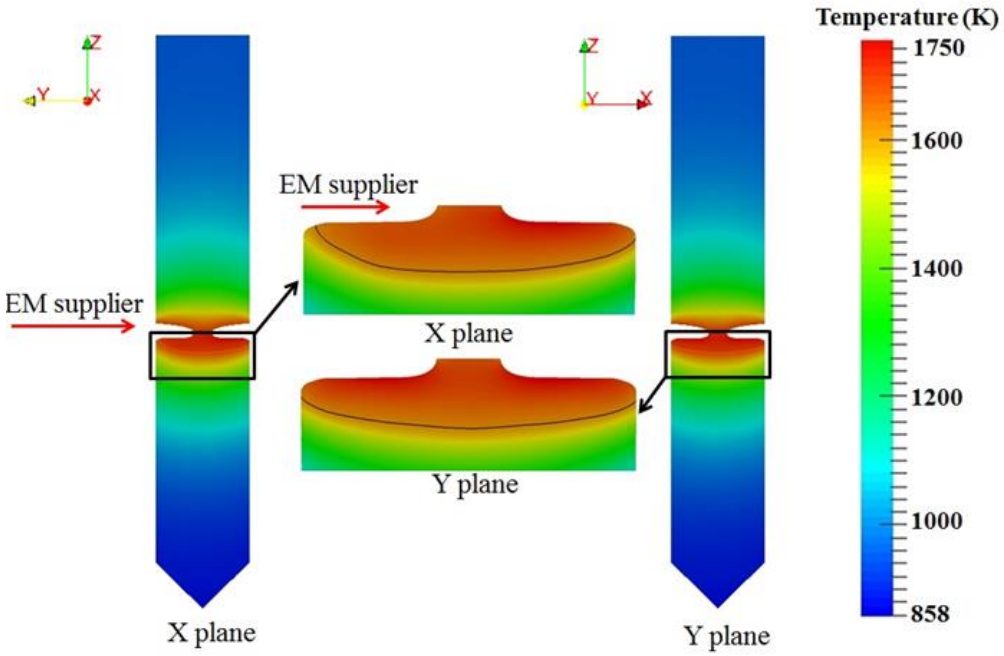

Fig.5 Temperature distribution at the cross section of X plane (left) and Y plane (right). Shape of solid-liquid interface at cross section of X plane (center top) and Y plane (center bottom).

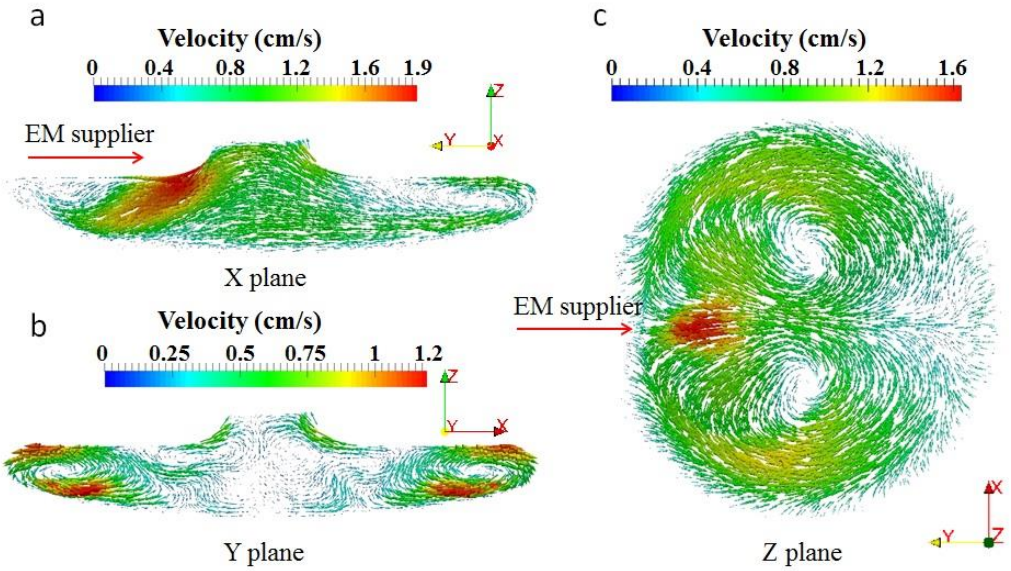

Fig.6 Velocity vector distribution of melt flow at the cross section: (a) X plane; (b) Y plane and at (c) Z plane.

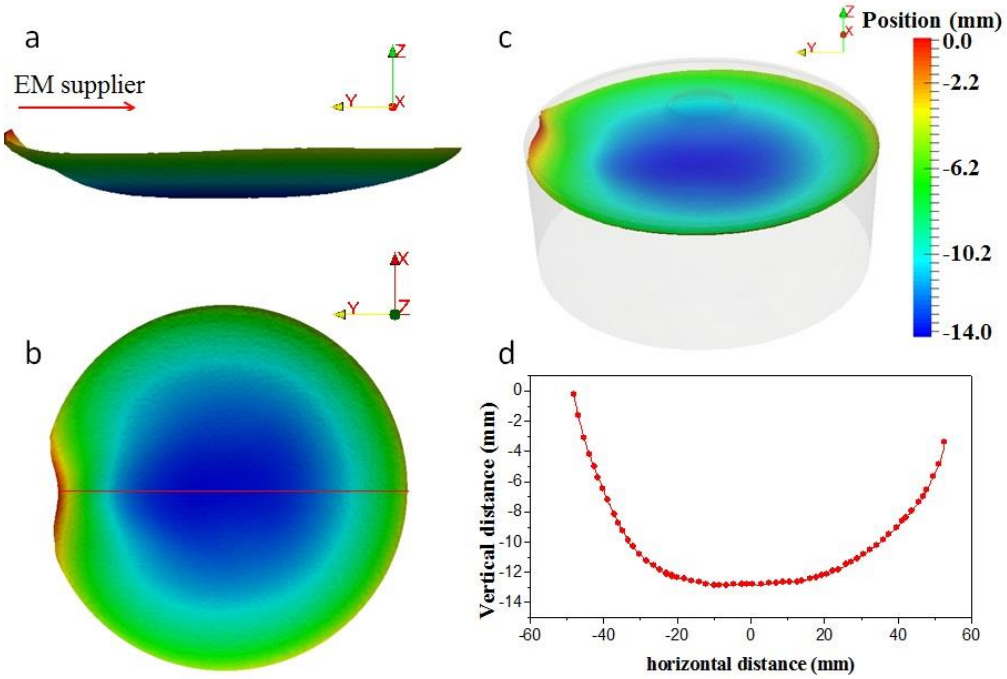

Fig.7 3D Shape of interface from different views: (a) front view; (b) isometric view; (c) top view. (d) Profile of interface coordinates along the line probe shown in (c).

velocity occurs at the position opposite the current supplier [see red circle in Fig. 4(a)] because of the high power density and high temperature of the melt at this position. The calculation shows that gas flow is asymmetric. Fig. 5 shows the temperature distribution in the feed rod, melt, and crystal: the lowest temperature occurs below the current supplier because the minimum heat power density induced by the EM field is at the free surface below the main slit [Fig. 3(c)]. Thus, the temperature distribution in the X plane is asymmetric. However, in the Y plane, the temperature distribution is symmetric because the current supplier has no effect there.

The results for the X plane [Fig. 6(a)] confirm that melt flows from the position opposite the current supplier to the position below the current supplier because of the buoyant flow caused by temperature difference. In the Y plane, there is no effect of current supplier, so the melt flow is symmetric as the temperature is symmetric. Moreover, two vortices are formed inside the melt. Marangoni effect caused a strong flow at the free surface of the melt. In Fig. 6(c), due to the buoyant force, the melt flows from the low-temperature zone to the high-temperature zone and then flows back to the low-temperature zone. This unique flow pattern is caused by the asymmetric temperature distribution.

From the calculated interface shape [Fig. 7(a)], it is observed that there is a bulge in the interface below the current supplier. This phenomenon is due to the low temperature of the melt below the current supplier. Fig. 7(b) and Fig. 7(c) show that the center of the interface is symmetric and not influenced by the asymmetric temperature distribution at the free surface. In the Fig. 7(d), the asymmetric interface during the growth process indicates that the growth rate is not homogenous. The rotation of crystal combined with the inhomogeneous growth rate would result in the striations inside the as-grown crystal.

4. Summary

3D global model of the FZ process including 3D EM model and 3D heat transfer model has been developed. The advantage of the new model is no assumption of axis-symmetry. The full 3D model is feasible to predict asymmetric mass transfer, heat transfer and solid-liquid interface. The model includes the effect of 3D gas flow on the temperature distribution in the feed rod, melt, and crystal. The steady calculation results show that asymmetric interface forms during the growth process caused by the asymmetric inductor. The improvement of the inductor design would significantly decrease the rotation striation of silicon crystal.

Acknowledgments

This work was partly supported by the New Energy and Industrial Technology Development Organization (NEDO) under the Ministry of Economy, Trade and Industry (METI).

References

1) B. Nacke and A. Muiznieks, GAMM-Mitteilungen 30, 113-124 (2007).
2) A. Van Run, J. Cryst. Growth 47, 680-692 (1979).
3) A. Mühlbauer, A. Muiznieks, J. Virbulis, A. Lüdge, and H. Riemann, J. Cryst. Growth 151, 66-79 (1995).
4) A. Mühlbauer, A. Muiznieks, G. Raming, H. Riemann, and A. Lüdge, J. Cryst. Growth 198, 107-113 (1999).
5) M. Wünscher, A. Lüdge, and H. Riemann, J. Cryst. Growth 318, 1039-1042 (2011).
6) M. Wünscher, R. Menzel, H. Riemann, and A. Lüdge, J. Cryst. Growth 385, 100-105 (2014).
7) A. Sabanskis, K. Surovovs, J. Virbulis, 3D modeling of doping from the atmosphere in floating zone silicon crystal growth, J. Cryst. Growth 457, 65-71 (2017).
8) A. Sabanskis, J. Virbulis, Simulation of the influence of gas flow on melt convection and phase boundaries in FZ silicon single crystal growth, J. Cryst. Growth 417, 51-57 (2015).
9) K. Surovovs, A. Muiznieks, A. Sabanskis, J. Virbulis, Hydrodynamical aspects of the floating zone silicon crystal growth process, J. Cryst. Growth 401, 120-123 (2014).
10) http://www.salome-platform.org/.
11) https://openfoam.org/release/2-3-1/.
12) P. Gresho, J. Derby, A finite element model for induction heating of a metal crucible, J. Cryst. Growth 85 (1987) 40-48.
13) http://www.openfoam.com/documentation/cpp-guide/html/guide-turbulence-ras-k-omega-sst.html.